

# Gaussian Process Mapping of Uncertain Building Models with GMM as Prior

Qianqian Zou<sup>1</sup>, Claus Brenner<sup>1</sup> and Monika Sester<sup>1</sup>

**Abstract**—Mapping with uncertainty representation is required in many research domains, such as localization and sensor fusion. Although there are many uncertainty explorations in pose estimation of an ego-robot with map information, the quality of the reference maps is often neglected. To avoid the potential problems caused by the errors of maps and a lack of the uncertainty quantification, an adequate uncertainty measure for the maps is required. In this paper, uncertain building models with abstract map surface using Gaussian Process (GP) is proposed to measure the map uncertainty in a probabilistic way. To reduce the redundant computation for simple planar objects, extracted facets from a Gaussian Mixture Model (GMM) are combined with the implicit GP map while local GP-block techniques are used as well. The proposed method is evaluated on LiDAR point clouds of city buildings collected by a mobile mapping system. Compared to the performances of other methods such like Octomap, Gaussian Process Occupancy Map (GPOM) and Bayesian Generalized Kernel Inference (BGKOctomap), our method has achieved higher Precision-Recall AUC for evaluated buildings.

## I. INTRODUCTION

The environment references are often applied to help an autonomous system, such as a robot or automated vehicle, to understand unknown complex scenes, and therefore, locate and navigate itself accurately and safely. However, the uncertainties of the maps greatly affect the performance of localization, navigation security and collision avoidance for the autonomous system. The environment information can be represented in a straightforward way like point clouds, structured maps, or abstract surface models [3]. The common maps are, e.g., the high-definition (HD) vector maps [1], acquired with high geometric and semantic accuracy, 2D or 3D-grids with occupancy probabilities, such as Octomaps [2], or 3D-City models with various level of details. Uncertainty sources in the environment map are inevitable due to, e.g. ambiguous environment information, sparsity, occlusions and noise in point clouds [4]. Hence, when the map is treated as an ideal perfect reference in localization and path-planning tasks without considering its quality, it can result in severe errors, e.g., the wrongly modelled occluded building facades might cause the deviation in pose estimation. Additionally, one may use multiple sensors to perceive the environment or has the demand of updating the existing maps with new data. In those scenarios, a good uncertainty measure of the maps created by different sensors and agents is essential

for data fusion and motion planning purposes [5]. Although many existing studies about uncertainty models are found in automated driving related fields, they are mostly for pose estimation. There is a lack of sufficient research about the accuracy and precision of the environment references.

In the field of simultaneous localization and mapping (SLAM), the uncertainty-aware tasks require a reasonable expression of map uncertainty. There are some existing methods estimating the uncertainty of maps to improve the localization accuracy or make the results more robust [3], [6], [7]. For example, Biber [6] proposed to represent the environment using normalization distribution transformation (NDT) maps, where the map uncertainty is measured by the distribution in the cell. However, it assumes independent discontinuous distributions of the neighboring cells and has been found to result in higher uncertainty at cell boundaries [8]. Ehsan [3] introduced the idea to build abstract vectors and planar surface maps of buildings and grounds, where the uncertainty is given by the normal distribution generated from vectors and planes. Building maps with fixed interval uncertainties are used in hybrid interval-probabilistic localization [7]. Occupancy maps with uncertain occupied cells are also widely used in localization, whose uncertainties are represented by the occupancy probabilities.

All these existing studies prove the importance of quantifying the uncertainty of maps. However, It remains challenging to map the continuous space from noisy sparse point clouds and equip the reasonable uncertainties to it. There is still a research gap for measuring the spatial uncertainty of maps in urban areas. There are many man-made structures with relative regular geometrical shapes, where buildings are often the most important ones for localization, e.g. as used in [3], [7]. A detailed spatial uncertainty representation of building models in urban scenes is of great interest to explore.

The choice of an adequate uncertainty measure in environment mapping is critical. To tackle this problem, the uncertainty and completeness of a map can be described in a probabilistic fashion. GP with its data-driven and probabilistic nature has proven to be a powerful tool for the quantification of uncertainty in various research fields. Dragiev [9] proposes the GP implicit surfaces for the object in the environment for efficient robot manipulation. Mouhyemen [10] combines a parametric model of the system with sparse GPs to capture unmodeled dynamics. The posterior mean and covariance kernel of a GP serve as the best estimation of the object and the uncertainty measure, respectively. GP Occupancy Mapping (GPOM) [11] demonstrates how to predict a continuous occupancy map from the sparse noisy

\*This work is supported by DFG Foundation

<sup>1</sup>Qianqian Zou, Claus Brenner and Monika Sester are with the Institut of Cartography and Geo-informatics in Leibniz University Hannover, Appelstraße 9a 30167 Hannover, Germany: {Qianqian.zou, Claus.brenner, Monika.sester}@ikg.uni-hannover.de.

point clouds with the non-parametric GP inference. The occupancy probability of unexplored space with no rays passing through or hitting are regressed by spatial neighbors in GP including well-calibrated uncertainties. It provides the possibility to capture the underlying correlation between spatially neighboring cells. The continuous inference gives the generalizability to building a map of desired resolutions in diverse applications. However, the drawback of GP lies in the expensive computational cost due to matrix inversion operations and this drawback limits the applicability of GP for large datasets. In order to achieve an acceptable computational efficiency, many approximation approaches such like the partition of spatial world into subsets, fusion of local GPs with Bayesian Committee Machine (BCM) or an sparse approximation of GPs have been proposed [10]–[14]. To avoid the unreliable prediction from successive BCM updates, Bayesian generalized kernel Octomap (BGKOctomap) [15] leverages Bayesian kernel inference and sparse kernels to perform a stable inference-based occupancy mapping. Jadidi [16] expanded the occupancy mapping to probabilistic geometric frontiers computed efficiently using the gradient of the GP occupancy map. Except for the efficiency, the occasional discontinuities in the environment can cause some troubles while the GP is often used for continuous targets. This effect is not well-studied in the current GP-based mapping.

There is another group of research learning structural surface models from measurements to probabilistically represent the perceived space. Thrun et al. [17] fitted a set of rectangular flat surfaces to compose three dimensional (3D) maps, with a group of parameters optimized by Expectation Maximization (EM) and the number of planes estimated by a Bayesian prior. With similar spirit but higher fidelity in approximating diverse arbitrary environments, Gaussian Mixture Models (GMMs) are employed as a semi-parametric tool with large numbers of components to extract the planar models [18] or obtain a high-fidelity representation of sensor observations [8], [19], estimating Gaussian mixtures instead of 3D planes. Nevertheless, the number of components has a great impact on the performance of GMM-based approaches and it is a non-trivial task to choose a proper number.

In this work, GP is used to obtain an inference-based surface model of structured buildings with GMM priors, leveraging the flexibility of non-parametric methods in arbitrary structures as well as the scalability of parametric approaches in large environments. When exploring large urban scenes, buildings are one of the most important structures for localization, which have relatively simple geometry and are easy to extract. GMM are first applied to extract the main planar surfaces with few components, while GPs are used to carve the irregular parts. In GP inference, the sets of local GPs corresponding to the certain planar objects are applied to adapt the discontinuities and reduce redundant computation, while the sparse kernel and data block partitioning techniques similar to the prior work [12], [13] are utilized to further improve the computational efficiency.

The contributions of this work are the following:

- We mapped uncertain building models in a probabilistic manner, which can be used in many down-stream tasks and updated probabilistically. This method aims to solve the problem of a lack of the uncertainty quantification for reference maps. The value of the uncertainty representation is revealed in the experiments when better results are obtained with only the accurate inference.
- GMM planes and local GP blocks are combined to yield a map with efficient surface prediction and maintain a good accuracy. Both GMM planes and GP function give a statistical uncertainty to the mapping process.
- We evaluate the mapping performance and the rightness of uncertainty description with real-world LiDAR point clouds of buildings, collected by mobile mapping system (MMS). The Precision-Recall curve and areas under curve (AUC) are used as the metric to evaluate the mapping results of Octomap, fast GPOM, BGKOctomap and our method. A comparison to the ROC AUC metric is also discussed.

The rest of the paper is structured as follows. Section II define the problem we aim to solve as well as the representation of building maps with uncertainty measures. In Section III, a brief introduction of the GMM and GP are presented. We explain how GPs are used to model non-planar surface with GMM prior to represent the uncertain building façade surface. The strategies for parameterizing the discontinuities, reducing computational efforts and outlier filtering are explained in detail. In Section IV, experiments using real LiDAR data collected by MMS are presented, where the qualitative results and qualitative evaluation with the state-of-art benchmarks are shown. Finally, we provide our conclusions and outlook for future work in Section V.

## II. PROBLEM STATEMENT

Concerning the problem of mapping uncertain building models as the premade map for an automotive robot in outdoor scenarios, we aim at offering a quantitative uncertainty measure to the building models, as shown in Figure 1. Considering that, sensors provide uncertain positions of points with noise and errors, this measure properly describes the quality of the map and is able to be refined or integrated with new data from subsequent measurement campaigns or from different sensors. As pre-processing work, classification of the raw measurements is performed to extract the building points for modelling.

Buildings consist of facades, with planar protrusions, extrusions, slopes (non-vertical planes, where the depth changes) and non-planar shapes. In the local frame of a façade, we consider the depth value over the façade plane as a continuous representation of the building surface. It is modelled with two parts: (1) regular planar parts are segmented by GMM; (2) each local GP is modelled in a planar segment to capture the arbitrary shapes.

The planar parts can be modelled with a few plane parameters and boundary points indicating the location and the shape of a local planar facet. Main façade plane, protrusions and extrusions can be specified with the corresponding

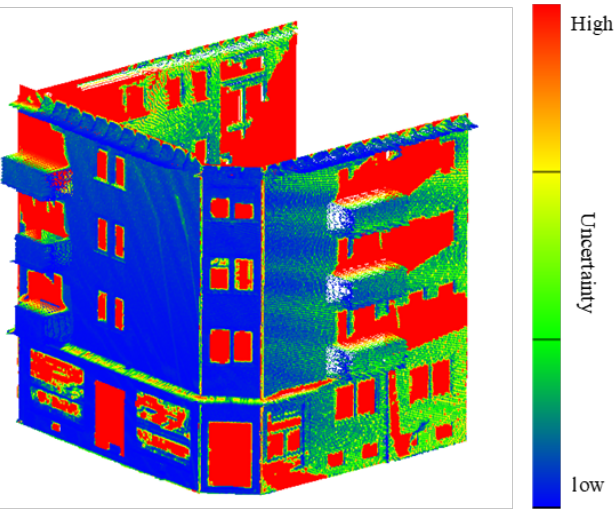


Fig. 1. Uncertain building model: colors indicate the uncertainty; redder colors denote high uncertainty.

plane layers resulting from a GMM. The remaining non-planar parts are represented as an implicit surface via non-parametric approaches. The local facet provides the prior information for modelling the non-planar points that fall into it. The parameters and boundary points of an extracted façade plane are given as prior; the non-planar surface on this plane can be represented with the GP function. In this case, a GP surface is a function telling the depth value of each location in space. A point  $x$  over plane has a distance  $s$  to the prior mean:

$$s = f(x) \begin{cases} = 0 & : \text{on the mean surface,} \\ < 0 & : \text{extrusion,} \\ > 0 & : \text{protrusion,} \end{cases} \quad (1)$$

This GP surface representation will provide an estimate of depth regarding the local planar segment at any location on the surface as well as the corresponding uncertainty of the estimation.

when counting all components, the surface depth is given by  $d$ :

$$d = g(x) + f(x|x \in G), \quad (2)$$

where  $g(x)$  is the expected plane depth from GMM results and  $f(x|x \in G)$  denoting the local implicit representation with regard to the planar component  $G$ .

### III. UNCERTAIN BUILDING SURFACE MODEL

In the following, we illustrate how the uncertain building models are represented probabilistically using GMM and GP. To generate uncertain building models, the building points are firstly extracted by the semantic classification from calibrated MMS point clouds. For each individual building, each facade plane will be extracted by the Random Sample Consensus (RANSAC) [20], where points are allocated to the corresponding facades. Then an uncertain model of facades can be explored.

#### A. Gaussian Mixture Model for planar surface

A façade is mainly composed of planar objects, which can be modelled by the plane normal, location and the boundary of the facets. The plane normal or the orientation of the building façade is determined by the third component of a principle component analysis (PCA). It serves as the depth direction, which decides the local frame of façade used in the following modelling. Many map representations such like 3D CityLoD2 models only map the building façade with one plane and ignore the extrusions and protrusions. The uncertainty is either not indicated or roughly one fitting standard deviation for the whole building façade. This is not sufficient for many tasks requiring high accuracy. In this paper, GMM is applied to cluster the points with different depth values to certain depth layers. Each depth layer is described by one Gaussian component in the GMM:

$$p(d) = \sum_{k=1}^K \pi_k \mathcal{N}(d|\mu_k, \sigma_k), \quad (3)$$

where  $d$  is the surface depth of a point,  $K$  is the number of Gaussian components;  $\{\pi_k, \mu_k, \sigma_k\}$  is a set of GMM parameters for the  $k$ -th depth layer –  $\pi_k$  is the prior probability or weight, meaning the importance of the component;  $\mu_k$  and  $\sigma_k$  are the mean and standard deviation of the Gaussian distribution.

The parameters  $\{\pi_k, \mu_k, \sigma_k\}_k^K$  are optimized by maximizing the log likelihood using EM algorithm. Figure 2 shows an example of the GMM results. The Gaussian component with the highest prior probability is the main façade plane.

Nevertheless, the limits of GMM are: 1) Non-planar surface cannot be modelled. 2) If the numbers of points on different layers have large disparities, meaning the training for different components is not balanced, the model might fail to model the small protrusions and extrusions. 3) Slopes might be simply modelled as a vertical plane. The non-parametric approach GP, on the other hand, is capable to model them with a data-driven nature. It is, therefore, introduced here to solve these problems mentioned above.

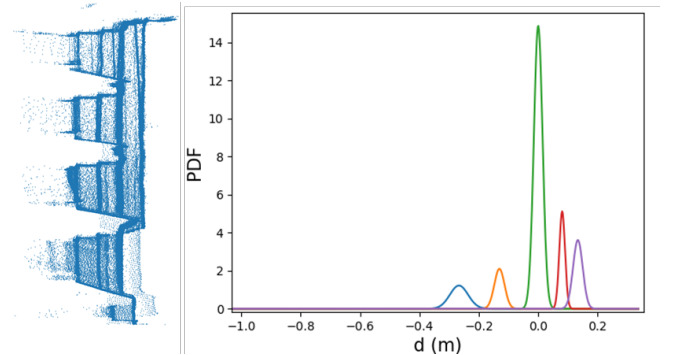


Fig. 2. GMM for plane modelling: the left picture is a façade profile; The Gaussian components (right) with different colors represent each depth layer. The one with highest peak is the main façade plane.

## B. Gaussian Process

A GP  $f(x) \sim GP(\mu(x), k(x, x'))$  is a popular Bayesian nonlinear regression method in machine learning. It can be seen as a multivariate normal distribution with infinite variables in a continuous domain, e.g. a continuous space. The distribution of any finite subset of those variables is still a joint Gaussian distribution. It is characterized by a mean function  $\mu(x)$  and a covariance function  $k(x, x')$ , which is also called kernel function. The prior GP mean function is often set to zero. There are many different kernel functions, and in this paper, automatic relevance determination (ARD) is used as the prior GP kernel function:

$$k_0(\mathbf{x}, \mathbf{x}') = \sigma_p^2 \exp\left(-\frac{1}{2} \sum_{m=1}^2 b_m (x_m - x_m')^2\right), \quad (4)$$

where  $l$  denotes the dimension of the input vector,  $\Theta = \{\sigma_p, b_1, b_2\}$  are the hyper-parameters for the kernel function, which are optimized by maximum likelihood given a measured dataset.

Provided a measurement dataset  $\mathcal{D} = (\mathbf{x}_i, y_i)_{i=1}^N$ , where  $\mathbf{X} = \{\mathbf{x}_i\}_{i=1}^N$  are  $N$  input vectors,  $\mathbf{y} = \{y_i\}_{i=1}^N$  are target values measured with noise  $\eta_i = \mathcal{N}(0, \sigma_\eta^2)$ , we have the likelihood as:

$$p(\mathbf{y}|\mathbf{X}, \Theta) = \mathcal{N}(\mathbf{y}|\mathbf{K}_N + \sigma_\eta^2 \mathbf{I}), \quad (5)$$

where  $\mathbf{K}_N = k_0(\mathbf{X}, \mathbf{X})$  is the covariance matrix of the input points with  $N \times N$  entries calculated by the prior kernel function

The rest of the space  $\mathbf{X}_*$  can be predicted with a multivariate Gaussian distribution conditioned on the observations  $\mathcal{D}$ . The posterior GP mean and kernel are calculated by [21]:

$$\mu(\mathbf{x}_*) = \mu_0(\mathbf{x}_*) + \mathbf{k}_*^T (\mathbf{K}_N + \sigma_\eta^2 \mathbf{I})^{-1} (\mathbf{y} - \mu_0(\mathbf{X})), \quad (6)$$

$$k(\mathbf{x}_*, \mathbf{x}'_*) = k_0(\mathbf{x}_*, \mathbf{x}'_*) - \mathbf{k}_*^T (\mathbf{K}_N + \sigma_\eta^2 \mathbf{I})^{-1} \mathbf{k}'_* + \sigma_\eta^2, \quad (7)$$

where the prior mean  $\mu_0(\mathbf{x})$  is set to zero,  $[\mathbf{k}_*]_N = k_0(\mathbf{X}, \mathbf{x}_*)$  and  $[\mathbf{k}'_*]_N = k_0(\mathbf{X}, \mathbf{x}'_*)$  are the prior covariance between the  $N$  input training points and the predicting points.

To utilize GP in generating an uncertain building model with dense point clouds, there are mainly two problems. First, mapping methods using GP have to consider the discontinuity of the environment while the GP often encodes the continuity and smoothness assumptions on targets. It is hard to model functions, which arbitrarily exhibit large derivatives, with a GP. Unfortunately, the large derivatives often appear in environment mapping. This issue is also addressed in [11], [13], where they tried special kernels to adapt the discontinuities, e.g. the Matérn covariance functions. However, the improvement is limited. Second, with large training datasets, the GP regression faces the computational problem due to the inversion matrix calculation  $O(N^3)$ . To capture the discontinuity and reduce the computational cost of GP in the case of a building model, two strategies applied here are: 1) using the GMM results as prior and 2)

partitioning data into blocks. These strategies are explained in detail in the following sections.

## C. GMM as Prior

Since buildings have relatively simple shapes with many planar objects, these planar parts can be modelled by a GMM as introduced in Section III. A. The estimated  $\mu$  are used as local prior GP means for modelling the remaining surface with non-planar points, points of non-horizontal normals and abnormal points too far away from the mean. In this way, the GMM information reduces the size of training points in GP. Additionally, the entire continuous space is divided into multiple local areas of GMM facets, modelled with GP-based approaches individually. This reduces the size of the kernel matrix. On the other hand, the planar segments with sharp depth variance compared to the neighboring regions cause the discontinuity on building surfaces. Another advantage of using GMM results as prior is to capture and parameterise the discontinuities on the facade surface. The independence can be introduced in different mean and covariance functions that are applied in different areas of the input locations.

The mean value of each Gaussian denotes the prior surface depth expectation of each planar layer, with standard deviation quantifying how precise and trustful the estimation is. The non-planar points which fall into a local facet on a certain layer are modelled by a local GP with this prior mean. The  $g(x)$  in Equation (2) is substituted by the mean  $\mu_k$  of a GMM component. The whole dataset is divided into subsets according to the results of GMM. Each local GP model has its own hyper-parameters and estimates the predictions only for the corresponding area.

Note that in the beginning, we had considered the weighted averaging operation for the small intersection area and the neighborhood of adjacent local segments, using BCM [22] or Product of Expert (PoE) [23]. However, there is no obvious improvement from the fusion and the decreased uncertainty after the mixture is not desired in our case. The efficiency is affected too. Thus, the mixtures of local GPs are not applied in this paper.

We categorize the points that cannot be well modelled by the GMM into: (1) non-planar points, (2) non-vertical slopes and (3) the points which are significantly excluded from their Gaussian distributions, i.e. not within the 95% confidence interval of the certain component. These points will be selected as training points and model the GP implicit surface as a function telling the continuous surface depth estimate. The points are selected according to the rules regarding the depth value  $d$  and the normal  $\mathbf{n} = \{n_x, n_y, n_d\}$ :

$$|d - \mu_k| > 1.96\sigma_k, \quad (8)$$

$$n_d(\mathbf{x}) < 0.9, \quad (9)$$

where  $\mu_k$  and  $\sigma_k$  are the parameters of the  $k$ -th Gaussian layer,  $n_d(\mathbf{x})$  is the component of the normal  $\mathbf{n}$ , which is perpendicular to the main façade plane.

Optimization of the parameters involves a reasonable

choice of the initial estimates. To speed up the learning process, these initial values are decided according to the following rules:

- The initial estimate for  $\sigma_p$  in the kernel of a local GP is set as the standard deviation of the corresponding planar patch  $\sigma_k$ ;
- The initial  $\{b_1, b_2\}$  are set to the same value, i.e. isotropic. We set  $\frac{1}{b_1} = \frac{1}{b_2} = 0.05m$ , observed from the investigation of the impact of the length-scale  $l = \frac{1}{b_1} = \frac{1}{b_2}$  on kernels and the learning samples;
- $\sigma_\eta$  reflects the precision of the sensors, point cloud alignment noise and random environmental noise. It is set based on the data situation. In this case,  $\sigma_\eta = 0.02m$ .

#### D. GP-block

Although we reduced the training points in the last section, the computational efficiency can be further improved by the data partitioning and GP-block techniques, which are inspired by [12]. In practice, the spatial correlation between two points decreases with their distance. This property is naturally captured by the length-scale hyper-parameter  $b$  in covariance functions of GPs. As the points far from each other have negligible influence that can be ignored in the covariance matrix, only close points have significant covariance and need to be considered in GP. An idea to exploit this property is to apply a sparse covariance function [14], making the covariance as zero when the distance is larger than a threshold. It also indicates the possible data partition of the training data. The entire training samples can be divided into some local blocks within a certain range, as employed in some GP mapping research [12], [13]. In those methods, the block size is set as the predefined scale value of the sparse kernel while in our case, the block size is determined by the distance corresponding to the threshold  $c_{min}$  of covariance values, calculated by Equation (4), when  $\sigma_p$  is temporarily set as 1 and  $b_1 = b_2 = b$ :

$$\exp\left(-\frac{1}{2} \sum_{m=1}^2 b(x_m - x'_m)^2\right) \geq c_{min}, \quad (10)$$

where  $c_{min} = 0.0001$  in this case. The block size is equal to  $|\mathbf{x} - \mathbf{x}'|$  when it makes the both sides equal. The extended block of a block is defined as the central block with its neighboring blocks. In GP regression, the points from the extended block are the training data for the central interested block.

#### E. Outlier filtering

To generate a GP inference robust to outliers, the model is required for outlier processing. There might be some outliers in the training samples due to false classifications (e.g. points of road signs in the vicinity of a building) or other unexpected reasons. In existing research [24]–[26], robust variants of GP regression have been proposed with long-tail distributions as the likelihood function instead of Gaussian noise, e.g. student-T distribution. However, the

Student-t likelihood can not be calculated in closed form in inference of the posterior [24], [26]. The alternative approach is to directly have a statistical test on a GP with Gaussian likelihood to check the probabilistic significance and identify the outliers, e.g. a Chi-squared test. In this work, the Chi-squared test with one degree of freedom is applied to remove outliers.

The procedure of outlier filtering is as follows.

1. The GP is trained normally with all training data and infers the mean and variance of each training point.
2. The Chi-squared test-statistic is calculated in Equation (11).
3. The test-statistics are compared to the  $\chi^2$  value given a certain  $\alpha$ -quantile level and the points with test-statistic values larger than  $\chi^2$  value will be removed as outliers.
4. Train the GP again with the filtered training data and predict the test points with mean and variance.

$$v_i^2 = \frac{(d_i - \mu_i)^2}{\sigma_i^2} \quad (11)$$

The above process may as well be repeated to iteratively trim the outliers, but the price will be more expensive cost of computation time. Therefore, in this case we only perform the test once in our experiment. The  $\alpha$ -percentile level in the test serves as a threshold to filter outliers, indicating the strictness of outlier detection. High values of  $\alpha$  will see many points as outliers, while a small  $\alpha$  gives more tolerance to the points deviating from the mean and might miss the outliers.

## IV. EXPERIMENTS AND EVALUATION

### A. Dataset

The GP-based implicit representation of a building surface is evaluated by the real-world LiDAR point clouds collected by a Riegl VMX-250 mobile mapping system for the urban environment, in Hanover, Germany. The scanner measurements of the system are specified as 5-mm precision, 10-mm accuracy. However, the accuracy of the GPS sensor in the system is much worse than the laser scanners. Point cloud alignment is thus used to correct the GPS trajectories in preprocessing and the data noise is given by a 2-cm standard deviation, resulting from the alignment [27]. In the experiments, only building points are of interests, which were extracted using the deep learning based method provided in [28]. In total, we used six measurement campaigns for the same urban areas collected from different dates to obtain very dense point clouds. Point clouds from one measurement campaign is used for modelling the uncertain map and the rest of data is used for testing and evaluation. In one single measurement campaign, the number of the points for one building façade depends on the building size and the measurement density. It is often larger than 10000, and can reach to a magnitude of 300000.

### B. Experiments

The building façades are firstly transformed individually to the local frame of their main planes, where a map point is a 2.5-dimensional point  $\mathcal{P} = \{\mathbf{x}, d\}$ , with the location

$x \in \mathbb{R}^2$  on the plane and the depth value  $d$  in the direction of the plane normal. The normal of the plane is derived by the PCA of all façade points. In the local façade frame, the planar points inside the 95% confidence interval are used as i.i.d. samples to optimize the parameters of GMM. Other points selected according to Equation (8) and (9) are used to derive the posterior GP-based inference models. The initial hyper-parameters are given based on the rules in Section III.C. Initial  $\sigma_\eta$  is 2-cm for this dataset.

Figure 3 is the qualitative result of modelled buildings with corresponding uncertainties. There are some occlusions in the original point cloud measurements, where the occluded surface is also inferred by the GP with high uncertainty (red). In the practical applications, users are able to select only the accurate part of maps or use the entire reference map with weights indicating the uncertainty.

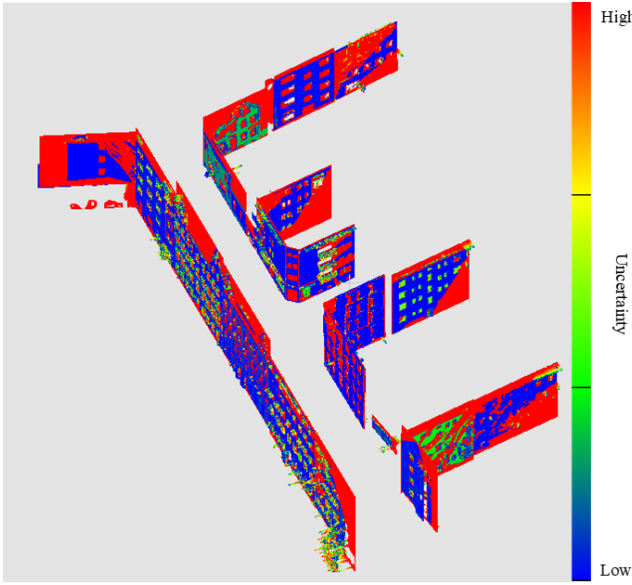


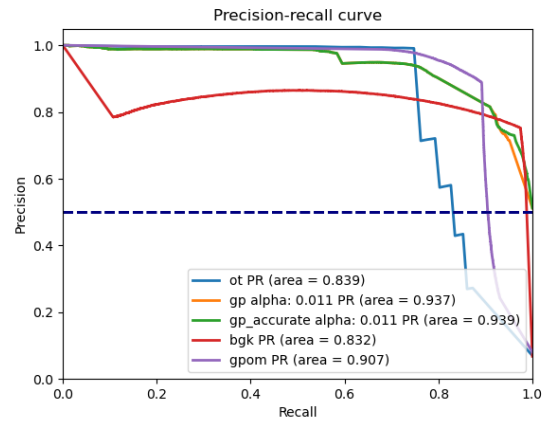
Fig. 3. Qualitative results of the uncertain building models: uncertainties of the modelling are denoted by colors. Redder colors indicate higher uncertainties while blue colors denote low uncertainties.

### C. Evaluation

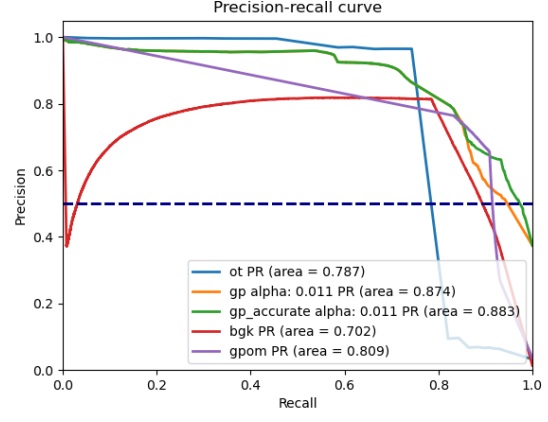
To evaluate the proposed method, the existing state-of-art approaches are used as benchmarks, i.e. Octomap [2], GPOM [13] and BGKOctomap [15]. Making the comparison possible, we first transform our abstract surface map to the 3D occupancy map, where probabilistic least-square classification is applied, inspired by the previous research [11], [12].

The metrics used for evaluation are: 1) Precision-Recall (PR) curves and 2) Areas under the curve (AUC). Note that some previous work used the receiver operation curve (ROC) and the corresponding AUC as the metrics. However, it is not proper to use ROC in highly-skewed data, where a large change in the number of false positives can only lead to a small change in the false positive rate used in ROC [29].

This occurs in our case, when the number of free samples is much larger than the number of occupied ones in outdoor scenarios. This issue is also addressed by the previous research [30]. Alternatively, PR-curve is more suitable for the highly imbalanced data [29] especially when the positive (occupied) case is of more concern. Precision compares the false positives with true positives, and Therefore, captures the detection errors of a large number of false positives. The goal of PR curves is to achieve the right-up corner instead of the left-up corner in ROC.



(a) Resolution: 0.1m



(b) Resolution: 0.05m

Fig. 4. PR curves and AUC comparison: the AUC value of each curve is given in the legend.

Figure 4 compares the AUC of different approaches modelling the space occupancy in two resolutions (0.1m and 0.05m). In general, GP inference-based maps have better performance, among which, our proposed method (green and orange curves) achieves the highest AUC values and is more robust to the small resolution. The green curves denote the case when we only consider the accurate inference of the map, i.e. areas with small uncertainty. The variance threshold is selected as 0.01 in this case. Areas with inference variance larger than 0.01 are seen as unknown. The figure shows that improvement is obtained by using only the accurate

parts and the corresponding maps (green curves) give the best performance. This shows the value of the uncertainty representation of maps and indicate the potential application of this uncertain model in the down-stream uncertainty-aware tasks.

## V. CONCLUSIONS

In summary, this paper proposed a method to generate building models as reference maps with associated uncertainty measures. The GMM and GP approaches are combined to map the planar parts and non-planar surface together. Local GP and data partition techniques are introduced in GP to reduce the computational cost and parameterizing the discontinuity of the building surface. In the experiments, the abstract surface map is transformed to the occupancy map using probabilistic least-square classification and compared with the benchmarks. The result evaluation shows that local GP with GMM prior strikes the highest AUC values, and with the variance threshold, the accurate inference gives even better performance. It shows the potential to work with uncertainty in the future applications.

The generated map will be applied in the localization tasks in the future and the positioning results will be compared with other methods, such as NDT-based localization. The approach also has large potential to be used for incrementally updating and refining existing models from new data or other sensors; this will also be studied in future work.

## ACKNOWLEDGMENT

This work was funded by the German Research Foundation (DFG) as a part of the Research Training Group GRK2159, “Integrity and collaboration in dynamic sensor networks” (i.c.sens).

## REFERENCES

- [1] Zhang, C., Liu, L., Xue, Z., Guo, K., Yang, K., Cai, R. and Li, Z., 2021, September. Robust LiDAR Localization on an HD Vector Map without a Separate Localization Layer. In 2021 IEEE/RSJ International Conference on Intelligent Robots and Systems (IROS) (pp. 5536-5543).
- [2] Hornung, A., Wurm, K.M., Bennewitz, M., Stachniss, C. and Burgard, W., 2013. OctoMap: An efficient probabilistic 3D mapping framework based on octrees. *Autonomous robots*, 34(3), pp.189-206.
- [3] Javannardi, E., Gu, Y., Javannardi, M. and Kamijo, S., 2019. Autonomous vehicle self-localization based on abstract map and multi-channel LiDAR in urban area. *IATSS research*, 43(1), pp.1-13.
- [4] R. Wang, J. Peethambaran and D. Chen, "LiDAR Point Clouds to 3-D Urban Models: A Review," in *IEEE Journal of Selected Topics in Applied Earth Observations and Remote Sensing*, vol. 11, no. 2, pp. 606-627, Feb. 2018.
- [5] Y. Huang and K. Gupta, "RRT-SLAM for motion planning with motion and map uncertainty for robot exploration," 2008 IEEE/RSJ International Conference on Intelligent Robots and Systems, 2008, pp. 1077-1082.
- [6] Biber, P. and Straßer, W., 2003, October. The normal distributions transform: A new approach to laser scan matching. In *Proceedings 2003 IEEE/RSJ International Conference on Intelligent Robots and Systems (IROS 2003)*(Cat. No. 03CH37453) (Vol. 3, pp. 2743-2748).
- [7] Ehambram, A., Jaulin, L. and Wagner, B., 2022. Hybrid Interval-Probabilistic Localization in Building Maps. *IEEE Robotics and Automation Letters*.
- [8] Srivastava, S. and Michael, N., 2018. Efficient, multifidelity perceptual representations via hierarchical gaussian mixture models. *IEEE Transactions on Robotics*, 35(1), pp.248-260.
- [9] S. Dragiev, M. Toussaint, and M. Gienger. "Gaussian process implicit surfaces for shape estimation and grasping." In 2011 IEEE International Conference on Robotics and Automation, pp. 2845-2850. IEEE, 2011.
- [10] K. Mouhyemen, A. Patel, and A. Chatterjee. "Multi-sparse gaussian process: Learning based semi-parametric control." In 2020 IEEE/RSJ International Conference on Intelligent Robots and Systems (IROS), pp. 5327-5334. IEEE, 2020.
- [11] O'Callaghan ST, Ramos FT. Gaussian process occupancy maps. *The International Journal of Robotics Research*. 2012 Jan;31(1):42-62.
- [12] Kim, S. and Kim, J., 2015. GPmap: A unified framework for robotic mapping based on sparse Gaussian processes. In *Field and service robotics* (pp. 319-332).
- [13] Wang, J. and Englot, B., 2016, May. Fast, accurate gaussian process occupancy maps via test-data octrees and nested bayesian fusion. In *2016 IEEE International Conference on Robotics and Automation (ICRA)* (pp. 1003-1010).
- [14] Melkumyan, A. and Ramos, F.T., 2009, June. A sparse covariance function for exact Gaussian process inference in large datasets. In *Twenty-first international joint conference on artificial intelligence*.
- [15] Doherty, K., Wang, J. and Englot, B., 2017, May. Bayesian generalized kernel inference for occupancy map prediction. In *2017 IEEE International Conference on Robotics and Automation (ICRA)* (pp. 3118-3124).
- [16] M. G. Jadidi, J. V. Miró, R. Valencia and J. Andrade-Cetto, "Exploration on continuous Gaussian process frontier maps," 2014 IEEE International Conference on Robotics and Automation (ICRA), 2014, pp. 6077-6082.
- [17] Thrun, S., Martin, C., Liu, Y., Hahnel, D., Emery-Montemerlo, R., Chakrabarti, D. and Burgard, W., 2004. A real-time expectation-maximization algorithm for acquiring multiplanar maps of indoor environments with mobile robots. *IEEE Transactions on Robotics and Automation*, 20(3), pp.433-443.
- [18] Marriott, R.T., Pashevich, A. and Horaud, R., 2018. Plane-extraction from depth-data using a Gaussian mixture regression model. *Pattern Recognition Letters*, 110, pp.44-50.
- [19] O'Meadhra, C., Tabib, W. and Michael, N., 2018. Variable resolution occupancy mapping using gaussian mixture models. *IEEE Robotics and Automation Letters*, 4(2), pp.2015-2022.
- [20] Schnabel, R., Wahl, R. and Klein, R., 2007, June. Efficient RANSAC for point-cloud shape detection. In *Computer graphics forum* (Vol. 26, No. 2, pp. 214-226).
- [21] C. E. Rasmussen, "Gaussian processes in machine learning," in *Summer School on Machine Learning*, pp. 63–71, Springer, 2003.
- [22] Liu H, Cai J, Wang Y, Ong YS. Generalized robust Bayesian committee machine for large-scale Gaussian process regression. In *International Conference on Machine Learning 2018 Jul 3* (pp. 3131-3140).
- [23] H., Geoffrey E. "Training products of experts by minimizing contrastive divergence". *Neural Computation*, 14 (8):1771–1800, 2002.
- [24] Martinez-Cantin, R., Tee, K. and McCourt, M., 2018, March. Practical Bayesian optimization in the presence of outliers. In *International conference on artificial intelligence and statistics* (pp. 1722-1731).
- [25] Li, Z.Z., Li, L. and Shao, Z., 2021. Robust Gaussian process regression based on iterative trimming. *Astronomy and Computing*, 36, p.100483.
- [26] Vanhatalo, J., Jylänki, P. and Vehtari, A., 2009. Gaussian process regression with Student-t likelihood. *Advances in neural information processing systems*, 22.
- [27] C. Brenner, Scalable estimation of precision maps in a mapreduce framework. In: *SIGSPACIAL '16: Proceedings of the 24th ACM SIGSPATIAL International Conference on Advances in Geographic Information Systems*, ACM Press, 2016, New York, USA.
- [28] T. Peters and C. Brenner, "Automatic Generation of Large Point Cloud Training Datasets Using Label Transfer." In: *39th Annual Scientific and Technical Conference of the DGPF eV*, in Vienna, Austria., 2019.
- [29] Davis, J. and Goadrich, M., 2006, June. The relationship between Precision-Recall and ROC curves. In *Proceedings of the 23rd international conference on Machine learning* (pp. 233-240).
- [30] Miao, Y., Hunter, A. and Georgilas, I., 2021. Parameter reduction and optimisation for point cloud and occupancy mapping algorithms. *Sensors*, 21(21), p.7004.